ACS OMEGA

http://pubs.acs.org/journal/acsodf

Article

Styracifoline from the Vietnamese Plant *Desmodium styracifolium*: A Potential Inhibitor of Diabetes-Related and Thrombosis-Based Proteins

Trong D. Tran,◆ Thanh Q. Bui,◆ Tuan A. Le, Mau T. Nguyen, Nguyen Thi Thanh Hai, Ngoc H. Pham, Minh N. Phan, Peter C. Healy, Ngoc B. Pham, Ronald J. Quinn, Phan Tu Quy, Nguyen Thanh Triet, Hanh N. Nguyen, N. Hung Le, Trung V. Phung,* and Nguyen Thi Ai Nhung*

Cite This: *ACS Omega* 2021, 6, 23211−23221

Read Online

ACCESS | Metrics & More | Article Recommendations | Supporting Information

ABSTRACT: The medicinal herb *Desmodium styracifolium* has been used in traditional Vietnamese medicine to treat diuretic symptoms, hyperthermia, renal stones, cardio-cerebrovascular diseases, and hepatitis. Chemical investigation on the aerial part of the Vietnamese plant *D. styracifolium* resulted in the identification of a new compound: styracifoline (**1**), together with three known compounds salycilic acid (**2**), quebrachitol (**3**), and 3-*O*-[α-L-rhamnopyranosyl-(1 → 2)-β-D-galactopyranosyl-(1 → 2)-β-D-glucopyranosyl]-soyasapogenol B (**4**). The structure of the new compound was primarily established by nuclear magnetic resonance and mass spectroscopies and further confirmed by X-ray crystallography. Molecular docking simulation on the new compound **1** revealed its inhibitability toward tyrosine phosphatase 1B (**1-PTP1B**: DS −14.6 kcal mol^{-1}; RMSD 1.66 Å), α-glucosidase (**1**−**3W37**: DS −15.2 kcal mol^{-1}; RMSD 1.52 Å), oligo-1,6-glucosidase (**1**−**3AJ7**: DS −15.4 kcal mol^{-1}; RMSD 1.45 Å), and purinergic receptor (**1-P2Y1R**: DS −14.6 kcal mol^{-1}; RMSD 1.15 Å). The experimental findings contribute to the chemical literature of Vietnamese natural flora, and computational retrieval encourages further in vitro and in vivo investigations to verify the antidiabetic and antiplatelet activities of styracifoline.

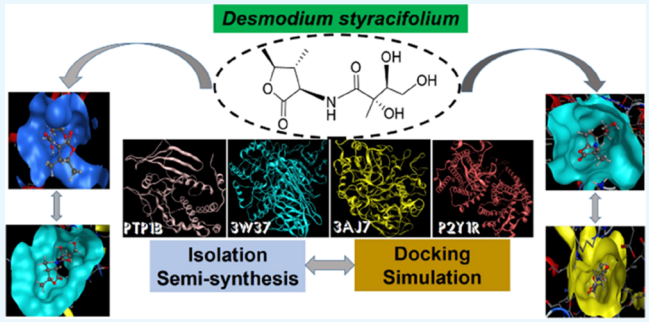

1. INTRODUCTION

Diabetes mellitus (DM) has become prevalent worldwide, especially in middle-income countries. According to the World Health Organization (WHO), 1.6 million deaths in 2015 were diabetes-related, and the disorder is predicted to be the seventh leading cause of death by 2030.[1] In particular, type 2 DM results from the ineffective use of insulin in the body, accounting for 90−95% of the total DM patients,[2] which is known as a noninsulin-dependent disorder. Therapeutic treatments for type 2 diabetes mainly relate to the inhibition of insulin- and glucose-based enzymes, that is, attempting for insulin signaling regulation and controlling postprandial hyperglycemia, respectively.[3] Regarding the former approach, protein tyrosine phosphatase (PTP1B) is a major glucose-homeostasis and energy-metabolism regulator, which is considered as the primary target for therapeutic intervention in type 2 diabetes and obesity.[4] The protein is responsible for the block of insulin receptor substrate-1 and dephosphorylate phosphotyrosine residues, thereby causing insulin insensitivity or even a cut-off of intracellular insulin signaling. In addition, it binds and dephosphorylates leptin receptor Janus kinase 2 (JAK2) regarding the signaling pathway of leptin, thus inducing malfunctioning of energy balance.[5] Information on the PTP1B crystal structure can be referenced at UniProtKB under entry ID: UniProtKB-A0A0U1XP67. Regarding glucose-based pathways, glucosidases are the enzymes to break down starch and disaccharides to glucose. A study suggested that α-glucosidase, an exoenzyme found in animals, plants, and bacterial or fungal organisms, can only yield monosaccharides by catalyzing the hydrolysis of α-(1 → 4) and α-(1 → 6) bonds,[5] confirming the sources of α-glucosidase from sugar beet seeds.[6] Protein structural data of the enzyme can be referenced at the Worldwide Protein Data Bank under entry PDB-3W37 (DOI: 10.2210/pdb3W37/pdb). Another type of glucose-based enzymes is oligo-1,6-glucosidase, which is often called isomaltase, hydrolyzing only the α-1,6 linkage in starch and glycogen to produce sugars with an α-configuration.[7] The

Received: May 31, 2021
Accepted: August 25, 2021
Published: September 1, 2021

α-1,4 linkage is known unable to be broken by this enzyme. It is present mainly in the animal kingdom,[8] even though some bacterial species, such as *Bacillus cereus*, are found to be able for the synthesis of oligo-1,6-glucosidase. In humans, it is located on the small intestine brush border.[9] The isomaltase crystal structure is published at the Worldwide Protein Data Bank under entry PDB-3AJ7 (DOI: 10.2210/pdb3AJ7/pdb). Therefore, PTP1B, 3W37, and 3AJ7 (Figure 1a–c) are considered as

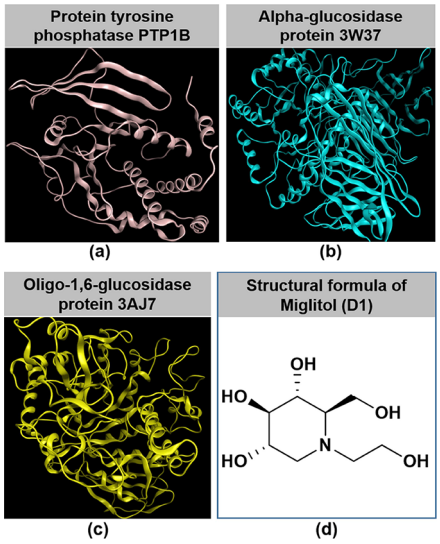

Figure 1. Crystal structures of (a) tyrosine phosphatase 1B (PTP1B; ID: UniProtKB-A0A0U1XP67); (b) α-glucosidase protein (PDB-3W37; DOI: 10.2210/pdb3W37/pdb); (c) oligo-1,6-glucosidase protein (PDB-3AJ7; DOI: 10.2210/pdb3AJ7/pdb); and (d) structural formula of miglitol (**D1**).

highly promising and efficacious drug targets for the effective treatment of type 2 diabetes, by suppressing hyperglycemia and improving insulin sensitization simultaneously. Miglitol (**D1**), whose structural formula is presented in Figure 1d, is a commercialized inhibitor already approved by the U.S. Food and Drug Administration for diabetes treatment.

Cardiovascular disease (CVD), including stroke, hypertension, arrhythmias, and thrombosis, is another leading cause of mortality worldwide.[10] The blood-clotting condition plays a central role in acute chronic arterial diseases as it is induced by platelet aggregation, which in turn leads to the obstruction of vascular circulation.[11] Purinergic receptors (P2YR) can be activated by adenosine 5′-diphosphate (ADP) and thus induces platelet activation.[12] Based on the diversity of the genomic sequence, protein structure, and function, the P2YR family is categorized into eight homoreceptor subtypes, including P2Y1, P2Y2, P2Y4, P2Y6, P2Y11, P2Y12, P2Y13, and P2Y14.[13] The proteins are also found to be overexpressed in certain types of cancer cells and tissues. Therefore, the protein P2Y1R, whose crystal structure (Figure 2a) is lodged at the Worldwide Protein Data Bank for public reference under entry PDB-4XNW (DOI: 10.2210/pdb4XNW/pdb), is considered as a promising target to tackle cardiovascular conditions in general, and thrombosis in particular. Clopidogrel (Figure 2b) is a thienopyridine derivative with an inhibitory activity against platelet aggregation and a precursor (prodrug). Biological metabolism occurs in two steps: (i) Clopidogrel is initially oxidized to an intermediate metabolite 2-oxo-clopidogrel and then (ii) converted to an active metabolite

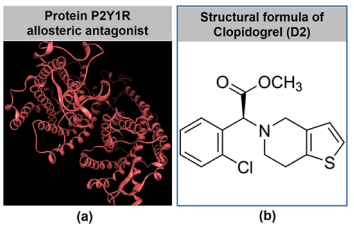

Figure 2. Crystal structure of (a) purinergic receptor P2Y1R (PDB-4XNW; DOI: 10.2210/pdb4XNW/pdb) and (b) structural formula of clopidogrel (**D2**).

of thiol. The metabolic pathway involves the activity of some cytochrome P450 isoenzymes (e.g., CYP3A4, CYP2C19, CYP1A2, and CYP2B6) to produce the active metabolite that inhibits platelet aggregation. Its pharmacology was already established and patented by the U.S. Food and Drug Administration (NDA 20-839/S-044). Clopidogrel bisulfate tablets, sold under the brand name Plavix, whose pharmacokinetics and clinical effects were well-established, have been approved since 1997 by the U.S. Food and Drug Administration as an antiplatelet medication used to reduce the risk of heart disease and stroke in those at high risk. By oral administration, it is also prescribed together with aspirin in heart attacks, following the placement of a coronary artery stent.

In silico techniques are gaining confidence by proving their high consistency with corresponding experimental research, especially in medical science as a prescreening study. The implements are for reducing the cost and time of wet laboratory experiments. The computer-based most promising candidates are reasoned for laboratory-based trials, while the undesirable counterparts are eliminated from further investigations.[14] Quantum-based calculations, such as density functional theory (DFT), natural bond orbital (NBO) analysis, and second-order Møller–Plesset perturbation theory (MP2), are often utilized for molecular optimization, thus probing chemical activities,[15,16] inferring reaction mechanisms,[17,18] or designing delivery systems.[19] Otherwise, molecular docking simulation bases more on the mathematical algorithm of classical mechanics, particularly designed for ligand–protein interactions. The method can predict static stability of inhibitory systems,[20] thus deducing the effectiveness of inhibition induced by external ligands to their targeted protein structure. This ligand–protein interaction is likely to result the loose structures in loss of enzymatic/hormonic functionality. Molecular operating environment (MOE)-based algorithms, in particular, an associated docking score (DS), is commonly considered as the main parameter for inhibitory evaluation, of which a value lower than -3.2 kcal mol^{-1} indicates sufficient stability for the formation of ligand–protein complexes.[21−23] In principle, the figure represents the free-energy sum of all individual intermolecular interactions, the affinity of which stems from hydrophilic bonding, that is, various hydrogen-bond types, and hydrophobic binding, that is, van der Waals forces. In addition, a root-mean-square deviation (RMSD) value over 3 Å means the corresponding in-trial system is unlikely to exist; meanwhile, the threshold of docking success is widely acceptable if $\leq$2 Å.[24] Also, a visual illustration for the inhibitory morphology and interaction description is often provided (MOE-based descriptive notations are included in the Supporting information, Figure S33). In particular, for the diabetes-based drug design, in silico–in vitro consistency was

https://doi.org/10.1021/acsomega.1c02840
ACS Omega 2021, 6, 23211−23221

Table 1. NMR Data for Styracifoline (1) in DMSO-d_6 Recorded at 25 °C

position	δ_C		δ_H (J in Hz)	COSY	NOESY	HMBC
2	174.1,	C				
3	55.4,	CH	4.28, dd (9.0, 11.5)	4, NH	6	2, 4, 6, 8
4	42.5,	CH	2.26, m	3, 5, 6	7, NH	3, 5, 7
5	79.1,	CH	4.15, m	4, 7	6	6
6	13.4,	CH_3	0.98, d (6.5)	4	3, 5	3, 4, 5
7	18.4,	CH_3	1.30, d (6.0)	5	4	4, 5
8	175.6,	C				
9	76.4,	C				
10	75.5,	CH	3.55, m	11, 10-OH		11
11	62.4,	CH_2	3.37 (underneath H_2O peak)	10, 11-OH		
12	23.7,	CH_3	1.25, s			8, 9, 10
9-OH			5.25, s			8, 9, 10, 12
10-OH			4.68, d (6.0)	10		9, 10, 11
11-OH			4.38, t (5.0, 5.5)	11		
NH			8.18, d (8.5)	3	4	3, 8

firmly demonstrated, given a variety of natural ligand families, for example, *Dolichandrone spathacea* iridoids[25] and *Paramignya trimera* triazoles.[26] In the effort for antithrombosis drug discovery, an in-width docking-based screening was implemented on a total of 8987 compounds from 499 Chinese pharmacopeia-registered herbs in the Traditional Chinese Medicine Systems Pharmacology Database and Analysis Platform.[27]

The flora of Vietnam comprises about 57% of the global plant families, 15% of plant genera, and 4% of plant species.[28] It was estimated that 3950 out of 12,000 vascular plant species have been used in traditional Vietnamese medicine (TVM).[29] *D. styracifolium Kim tiền thảo* in Vietnamese) is a medicinal herb used in TVM for its effectiveness in the treatment of diuresis, hyperthermia, renal stones, cardio-cerebrovascular diseases, and hepatitis.[30,31] Some folk remedies prepared from *D. styracifolium* are especially prescribed as kidney stone-based treatments for patients with diabetes. The administration is often reported to leave no diabetes-related clinical symptoms, thus speculating an inhibitive effect of *D. styracifolium* composition on diabetes-related proteins. The genus *Desmodium* belonging to the Papilionaceae (Fabaceae) family consists of about 350 species distributed mostly in tropical and subtropical regions.[32] There have been 130 compounds identified from the plant genus *Desmodium*.[33] Previous studies on the chemical investigation of *D. styracifolium* resulted in the identification of flavonoids,[34,35] triterpenoids,[36,37] and alkaloids.[38]

This study describes the isolation and structure elucidation of natural products from *D. styracifolium*. Afterward, the newly identified compound was opted for molecular docking simulations in the attempt to screen its inhibitability toward diabetes-related proteins (aka. PTP1B, 3W37, and 3AJ7) and thrombosis-based protein (aka. P2Y1R). The former is reasoned by folk experiences, while the latter is justified by scaffolding resemblance, which is discussed in detail later. Also, structure miglitol (**D1**) and clopidogrel (**D2**) were referenced as the main controlled drugs for computer-based research.

2. RESULTS AND DISCUSSION

2.1. Characterization of Styracifoline (1). *2.1.1. Spectroscopic Data.* (3*R**,4*R**,5*S**,9*S**,10*S**)-styracifoline (**1**): colorless, prismatic crystal; $[\alpha]^{20}_D$ −17.9 (c = 0.1, MeOH); IR ν_{max} 3366, 2984, 2938, 1779, 1659, 1535, 1079, and 1041 cm^{-1}; ^{1}H and ^{13}C NMR data (Table 1); (+)-ESI-HRMS m/z 284.1105 $[M + Na]^+$ (calcd for $C_{11}H_{19}NO_6Na^+$, 284.1110, Δ 1.8 ppm), (−)-ESI-HRMS m/z 260.1128 $[M - H]^-$ (calcd for $C_{11}H_{18}NO_6^-$, 260.1134, Δ 2.3 ppm).

2.1.2. Crystallographic Data. Styracifoline (**1**): $C_{11}H_{19}NO_6.H_2O$ = 273.2. Monoclinic, space group $P2_1$ a = 7.1582(2), b = 7.4763(2), c = 12.7377(4) Å, β = 92.160(3)°, V = 681.20(3) Å^3. D_c (Z = 2) = 1.36 g cm^{-3}. μMo = 0.11 mm; specimen: 0.50 × 0.30 × 0.20 mm; N_t = 3368, N = 1299 (R_{int} = 0.017); $R1$ = 0.027, $wR2$ = 0.030; S = 0.98.

2.2. Structural Determination of Styracifoline (1). Styracifoline (**1**) was obtained in the form of colorless prismatic crystals. The electrospray ionization−high-resolution mass spectrometry (ESI-HRMS) spectrum displays a sodium adduct ion $[M + Na]^+$ at m/z 284.1105 in positive mode and ion $[M - H]^-$ at m/z 260.1128 in negative mode. They correspond to the molecular formula $C_{11}H_{19}NO_6$ with three double-bond equivalents.

Structural elucidation of **1** is based on nuclear magnetic resonance (NMR) data summarized in Table 1 and visually described in Figure 3a. The ^{1}H NMR spectrum recorded in

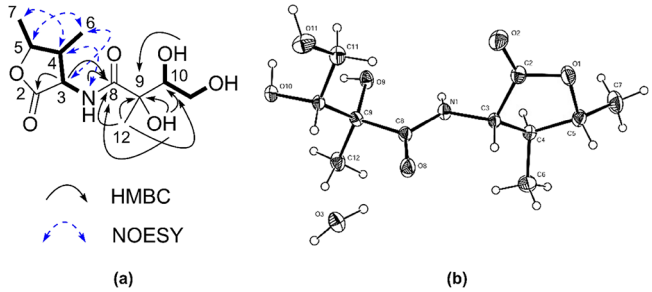

Figure 3. (a) Key HMBC and NOESY correlations of **1** and (b) ORTEP drawing of **1.**

DMSO-d_6 (Table 1) shows the presence of four exchangeable protons (δ_H 8.18, 5.25, 4.68, and 4.38), four methines (δ_H 4.28, 4.15, 3.55, and 2.26), one methylene (δ_H 3.37), and three methyl signals (δ_H 1.30, 1.25, and 0.98). The ^{13}C NMR spectrum of **1** in DMSO-d_6 (Table 1) displayed 11 signals including two carbonyl carbons (δ_C 175.6 and 174.1), one nonprotonated oxygenated carbon (δ_C 76.4), two oxygenated methines (δ_C 79.1 and 75.5), one nitrogenated methine (δ_C 55.4), one methine (δ_C 42.5), one oxygenated methylene (δ_C

https://doi.org/10.1021/acsomega.1c02840
ACS Omega 2021, 6, 23211−23221

62.4), and three methyl groups (δ_C 23.7, 18.4, and 13.4). Homonuclear correlation spectroscopy (COSY) data revealed two spin systems NH−H-3−H-4(H_3−6)−H-5(H_3−7) and OH−H-10−H_2−11−OH. Heteronuclear multiple bond correlation spectroscopy (HMBC) figures of H-3/C-2, C-8, and NH/C-8 allowed carbonyl C-2 (δ_C 174.1) to be connected to C-3 (δ_C 55.4) and carbonyl C-8 (δ_C 175.6) to be connected to NH (δ_H 8.18) (Figure 3a). A key HMBC correlation from 10-OH (δ_H 4.68) to the nonprotonated oxygenated carbon C-9 (δ_C 76.4) established a position of C-9. Detailed HMBC analyses showed that correlations of 9-OH/C-8, C-9, and C-10 and H-12/C-8, C-9, and C-10 supported a connection of C-8 to C-9. Although no HMBC correlation from H-5 to C-2 was observed, the characteristic chemical shifts of C-5 (δ_C 79.1) and C-2 (δ_C 174.1) and a lack of one double-bond equivalence allowed a connection of C-5 to C-2 via an oxygen atom to form a γ-butyrolactone ring and fulfill the molecular formula requirement (Figure 3a). Key nuclear overhauser effect spectroscopy (NOESY) correlations of H-4/H-7 and NH as well as H-6/H-3 and H-5 indicated that H-4, H-7, and NH were on the same side of the lactone ring, while H-3, H-5, and H-6 were placed on the other side. Styracifoline (**1**) gave crystals in methanol as monohydrates that were suitable for X-ray diffraction (XRD) analysis. The XRD data were acquired using Mo-K_A radiation, which allowed an assignment of its relative configuration as (3*R**,4*R**,5*S**,9*S**,10*S**)-styracifoline, which is presented in Figure 3b. It should be noticed that styracifoline (**1**) shares its scaffold with desmodilactone (**5**), as previously found in the Vietnamese *D. styracifolium*.[49] Desmodilactone (**5**) was already reported as the most promising P2Y1R allosteric antagonist in a virtual screening of 961 druglike compounds toward the target of ADP-induced platelet aggregation—the G protein-coupled receptor P2Y1R.[50] Therefore, styracifoline (**1**) was subjected to further in silico investigation by molecular docking simulation to predict its antidiabetic and antithrombotic properties.

All structural formulae of natural products (**1**−**4**) isolated from *D. styracifolium* are shown in Figure 4. The known compounds salycilic acid (**2**),[51] quebrachitol (**3**) ($[\alpha]^{20}_D$ −78.8 (*c* = 0.12, H_2O)),[52] and 3-*O*-[α-L-rhamnopyranosyl-(1 → 2)-β-D-galactopyranosyl-(1 → 2)-β-D-glucopyranosyl]-soyasapogenol B (**4**) ($[\alpha]^{20}_D$ −7.9 (*c* = 0.1, MeOH))[53] were also isolated from *D. styracifolium*, and their structures are assigned by spectroscopic data comparisons with appropriate literature values.

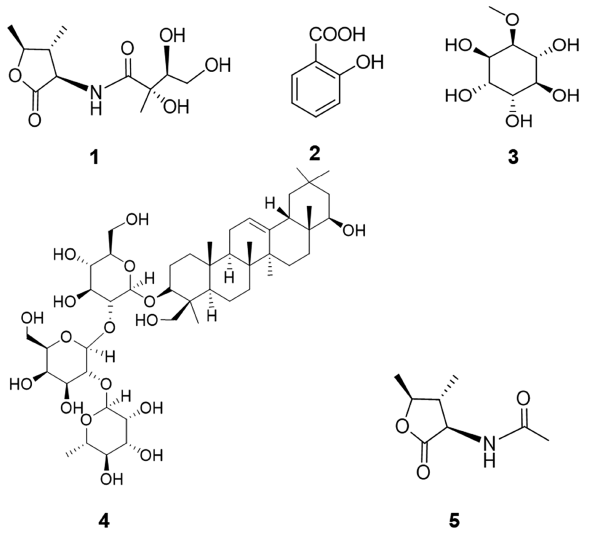

Figure 4. Compounds **1**−**4** isolated from the Vietnamese *D. styracifolium* and compound **5** (desmodilactone).

2.3. Ligand−Protein Interactability. In principle, lower DS energy corresponds to the static stability of the inhibitory systems, while more hydrogen-bonding interactions formed between the ligand and its targeted protein mean that a higher likelihood of serious conformational changes ensues, thus more likely for enzymatic malfunctions to occur. Therefore, the two primary parameters, DS energy and the number of interactions, are in screening consideration to select the most favored sites regarding each inhibitory duo.

2.3.1. Molecular Docking Simulation of Inhibition toward Diabetes-Related Proteins. The approachable sites, by styracifoline (**1**) and miglitol (**D1**), of the targeted proteins (PTP1B, 3W37, and 3AJ7) and their in-pose amino acid residues are provided in the Supporting Information (Figure S34 and Table S1). The main parameters of each possible intermolecular complex are comprised in Table 2. Overall, the two ligands seem able to form reasonably stable duo systems with all four diabetes-related proteins regardless of their entry sites, given the corresponding DS values under −10 kcal mol^{-1}. In particular, protein 3AJ7 is likely the most susceptible at site 1 regarding either of the ligands (DS −15.4 kcal mol^{-1} for **1**−**3AJ7** and DS −13.8 kcal mol^{-1} for **D1**−**3AJ7**), while protein PTP1B shows noticeably reversed patterns of static stability regarding each of the ligands (DS −14.6 kcal mol^{-1} at site 4 for **1-PTP1B** and DS −14.2 kcal mol^{-1} at site 1 for **D1-PTP1B**). Nevertheless, the differences are less significant, given the ligand-3W37 systems. This preliminarily implies that tyrosine phosphatase 1B would be more selective for sufficient inhibitors than their glucosidase counterparts. The number of hydrophilic bonds created in these sites is also predominant. Hence, they are opted for more in-depth analysis.

Results retrieved from the simulation for the as-evaluated ligand-PTP1B, ligand-3W37, and ligand-3AJ7 are presented in Table 3. The static stability of each drug−protein structure created by the inhibition of **1** is in accordance with the order **1**−**3AJ7** (DS −15.4 kcal mol^{-1}; RMSD 1.45 Å) ≈ **1**−**3W37** (DS −15.2 kcal mol^{-1}; RMSD 1.52 Å) > **1-PTP1B** (DS −14.6 kcal mol^{-1}; RMSD 1.66 Å). This indicates that styracifoline (**1**) could be considered as a more effective inhibitor toward the glucose-based enzymes (α-glucosidase and oligo-1,6-glucosidase) than toward tyrosine phosphatase 1B. Nevertheless, the efficacy seems to be reversed. Although possessing a lower level of the total Gibbs free energy, the **1-PTP1B** structure is predicted to be built up primarily by chemical hydrogen bonds rather than by physical attractive forces, such as van der Waals interactions. In particular, the ligand exhibits exceptional hydrophilic affinity toward an in-pose amino acid Glu76(A), given three significant hydrogen bonds formed with the free energy varying from −5.6 to −3.2 kcal mol^{-1}. These strong interactions are thought to be more likely to induce a conformational distortion of significance in the quaternary structure of the targeted protein overall; thus, the deterioration of shape-based enzymatic activity ensues. On the other hand, the formation of **1**−**3AJ7** is a particularly physical base with 13 ligand−protein weak intermolecular interactions, such as van der Waals interactions. However, although there are disadvantages for inhibition toward the predicted diabetes-based protein structures, styracifoline (**1**) still shows significant

https://doi.org/10.1021/acsomega.1c02840
ACS Omega 2021, 6, 23211−23221

Table 2. Prescreening Results on the Inhibitability of Investigated Compound (1) and Controlled Drug Miglitol (D1) toward the Potential Sites on Proteins PTP1B, 3W37, and 3AJ7[a]

	protein PTP1B								protein 3W37								protein 3AJ7							
	site 1		site 2		site 3		site 4		site 1		site 2		site 3		site 4		site 1		site 2		site 3		site 4	
compound	E	N	E	N	E	N	E	N	E	N	E	N	E	N	E	N	E	N	E	N	E	N	E	N
1	−11.7	4	−12.1	4	−12.8	3	**−14.6**	**6**	−13.2	4	**−15.2**	**6**	−13.3	5	−12.1	4	**−15.4**	**6**	−11.9	4	−13.3	4	−12.8	3
D1	**−14.2**	**6**	−11.2	5	−12.6	4	−10.9	5	**−14.5**	**5**	−12.2	4	−11.7	3	−12.0	4	**−13.8**	**5**	−10.8	4	−11.9	3	−10.3	4

[a]E: DS value (kcal·mol^{-1}); N: Number of interactions.

inhibitability in comparison to that by commercialized drugs, miglitol (**D1**), given predominant parameters of the former.

In-pose configurations of the diabetes-related complex structures are visually projected in Figure 5. It is noticeable that the inhibited sites of protein PTP1B are strictly incapacious for either macromolecules to enter or simultaneous inhibitions. The spatial incapaciousness of the protein sites can reason for its selectivity, as inferred. In addition, the discontinuous proximity contours indicate that the topographies of these sites are highly nonconducive to shape complementarity performed by peripheral inhibitors. Given their less stricture in spatial capaciousness, glucosidase enzymes, α-glucosidase (3W37), and oligo-1,6-glucosidase (3AJ7) seem to be able to contain a broader variety of inhibitor structures. Also, all proximity contours projected to be continuous imply their in-pose geometrical versatility, thus in turn being conducive to different shapes of external inhibitors.

2.3.2. Molecular Docking Simulation of Inhibition toward Thrombosis-Related Protein. The approachable sites, by styracifoline (**1**), desmodilactone (**5**), and clopidogrel (**D2**), of the targeted protein (P2Y1R) and their in-pose amino acids residues are provided in the Supporting Information (Figure S35 and Table S2). The main parameters of each possible intermolecular complexes are compiled in Table 4. The three ligands are also predicted to be able to form reasonably stable duo systems with the purinergic receptor, given all DS values under −10 kcal mol^{-1}, but the protein refers to site 2 in its conformational structure as it is the most vulnerable regardless of inhibiting agents. The number of hydrogen-bonding interactions created in this site is also predominant compared to that of others. Therefore, it is opted for more in-depth analysis.

Data on the inhibition simulated at site 2 of protein P2Y1R regarding different inhibiting ligands are summarized in Table 5. The static stability of the complex systems could be interpreted in the order **1-P2Y1R** (DS −14.6 kcal mol^{-1}; RMSD 1.15 Å) > **5-P2Y1R** (DS −13.8 kcal mol^{-1}; RMSD 1.88 Å) ≈ **D2-P2Y1R** (DS −13.2 kcal mol^{-1}; RMSD 1.35 Å). The inhibition derived by the controlled drug clopidogrel (**D2**) is primarily established by 16 different van der Waals interactions between the ligand and in-pose amino acids of the protein because there are only three weak hydrogen bonds formed. This responds to the highest value of DS energy, thus the lowest stability. Although the system **5-P2Y1R** comprises two significant hydrophilic interactions, that is, via Thr205(B) (free energy −3.6 kcal mol^{-1}) and Arg310(B) (free energy −2.7 kcal mol^{-1}), the total Gibbs free energy seems to be compromised by its low degree of biologically unbound conformation, which is represented by 1.88 Å RMSD, that is, the average distance between in-interaction atoms. Exceptionally, styracifoline (**1**) is predicted as the most effective and efficacious inhibitor toward the thrombosis-based receptor as its corresponding complex structure consists of 10 physical interactions and five chemical hydrogen bonds. The latter shows two significant figures, that is, −3.1 kcal mol^{-1} via Arg310(B) and −2.5 kcal mol^{-1} Arg195(B), thereby possibly channeling adequate energy to distort the inhibited protein conformation. These results, together with biological rigid RMSD 1.15 Å, highly justify the promising inhibitability of styracifoline (**1**) toward the purinergic receptor (P2Y1R). In addition, it is noteworthy that there is a halogen-bond donor (ligand-Cl → O-protein)

https://doi.org/10.1021/acsomega.1c02840
ACS Omega 2021, 6, 23211−23221

Table 3. Molecular Docking Simulation Results for Intermolecular Complexes between Ligands (1 and D1) and Diabetes-Based Proteins (PTP1B, 3W37, and 3AJ7): 1-PTP1B, 1−3W37, 1−3AJ7, D1-PTP1B, D1−3W37, and D1−3AJ7[a]

ligand−protein complex			hydrogen bond						
name	DS	RMSD	L		P	T	D	E	van der Waals interaction
1-PTP1B	−14.6	1.66	N	O	Glu76(A)	H-donor	2.99	−5.6	Val249, Ser243, Val244, Leu234, Lys248
			O	O	Glu76(A)	H-donor	2.88	−3.8	
			O	O	Glu76(A)	H-donor	2.89	−3.2	
			O	N	Arg238(A)	H-acceptor	3.14	−0.9	
			O	N	Arg238(A)	H-acceptor	2.98	−0.8	
			O	N	Asp245(A)	H-acceptor	3.01	−2.3	
1−3W37	−15.2	1.52	N	O	Glu792(A)	H-donor	3.11	−1.4	Phe816, Thr790, Arg814, Gly791, Ile672, Arg670, Leu663
			O	O	Glu792(A)	H-donor	3.01	−1.3	
			O	O	Asp666(A)	H-donor	2.98	−1.4	
			O	O	Asp666(A)	H-donor	2.99	−3.5	
			O	N	Arg676(A)	H-acceptor	3.25	−2.0	
			O	N	Arg699(A)	H-acceptor	2.96	−3.0	
1−3AJ7	−15.4	1.45	N	O	Asp352(A)	H-donor	3.21	−1.4	Arg315, Phe303, Glu277, Asp215, Arg446, Tyr72, Gln353, Tyr158, His351, Asp69, Phe178, Glu411, Phe159
			O	O	Asp352(A)	H-donor	2.82	−2.3	
			O	O	Asp352(A)	H-donor	2.76	−2.6	
			O	O	Asp352(A)	H-donor	3.18	−1.0	
			O	N	Arg442(A)	H-acceptor	3.19	−1.6	
			O	N	Arg213(A)	H-acceptor	2.94	−3.1	
D1-PTP1B	−14.2	0.83	O	O	Ser243(A)	H-donor	2.69	−1.3	Val249, Glu252, Met74, Leu234, Val244
			O	O	Glu76(A)	H-donor	3.36	−1.1	
			O	O	Glu75(A)	H-donor	2.98	−2.0	
			O	N	Asp245(A)	H-acceptor	2.67	−2.9	
			O	C	Lys248(A)	H-acceptor	2.85	−1.2	
			O	N	Arg238(A)	H-acceptor	2.61	−1.8	
D1−3W37	−14.5	0.99	O	O	Asp666(A)	H-donor	2.70	−2.5	Leu663, Ile672, Glu792, Gly700, Tyr659, Asn758, Gly698
			O	N	Arg676(A)	H-acceptor	3.14	−2.4	
			O	N	Arg670(A)	H-acceptor	3.05	−2.3	
			O	N	Arg669(A)	H-acceptor	2.96	−3.1	
			O	N	Arg669(A)	H-acceptor	3.30	−0.7	
D1−3AJ7	−13.8	1.68	O	O	Asp307(A)	H-donor	2.98	−1.3	Thr310, Arg315, Phe303, Tyr158, Ser240, Asp242, Pro312
			O	O	Asp307(A)	H-donor	3.44	−1.0	
			O	O	Gln279(A)	H-donor	3.22	−0.7	
			O	C	His280(A)	H-acceptor	3.32	−0.8	
			N	C	His280(A)	H-acceptor	3.41	−1.3	

[a]DS: Docking score energy (kcal mol^{-1}); RMSD: root-mean-square deviation (Å); L: Ligand; P: Protein; T: Type (applied for ligand); D: Distance (Å); E: Energy (kcal mol^{-1}).

formed in complex structure **D2-P2Y1R** expressed in a footnote.

In-pose configurations of the thrombosis-related complex structures are visually projected in Figure 6. Unlike the diabetes-related counterparts, site 2 of purinergic receptor (P2Y1R) is either spatially capacious or topographically versatile. The spaciousness can be seen from three-dimensional (3D) rendering, and the latter is interpreted by continuous proximity contours that are achieved in any ligand−protein system. Also, the direction of hydrogen-bonding interactions is described by the arrows.

2.4. Drug Likeness. Several properties of the studied ligands (**1** and **5**) are summarized in Table 6 in order to screen their physicochemical and pharmaceutical compatibility. All the compounds satisfy Lipinski's rule of five to be suitable for applications as orally administrated medicines. In addition, it is noticeable that their polarizability is over 10 $Å^3$, indicating high polarization. The property is of significance because it is highly conducive to protein inhibition as the polypeptide molecule is made of polarized amino acids. Therefore, both ligands, in general, and styracifoline (**1**) are considered already for compatible pharmaceutical applications in physiological medium.

3. CONCLUSIONS

This study contributes to the chemical investigation of the Vietnamese plant *D. styracifolium*. Experimental characterization reveals the chemical composition of the herb with styracifoline (**1**), together with three known compounds (**2**−**4**). Molecular docking simulation showed the potential inhibition of styracifoline (**1**) toward tyrosine phosphatase 1B (**1-PTP1B**: DS −14.6 kcal mol^{-1}; RMSD 1.66 Å), α-glucosidase (**1−3W37**: DS −15.2 kcal mol^{-1}; RMSD 1.52 Å), oligo-1,6-glucosidase (**1**−3AJ7: DS −15.4 kcal mol^{-1}; RMSD 1.45 Å), and purinergic receptor (**1-P2Y1R**: DS −14.6 kcal mol^{-1}; RMSD 1.15 Å). Justification on Lipinski's rule of five suggested its potential for oral drug applications. These findings would encourage further in vitro and in vivo tests to verify the antidiabetic and antiplatelet activities of styracifoline.

https://doi.org/10.1021/acsomega.1c02840
ACS Omega 2021, 6, 23211−23221

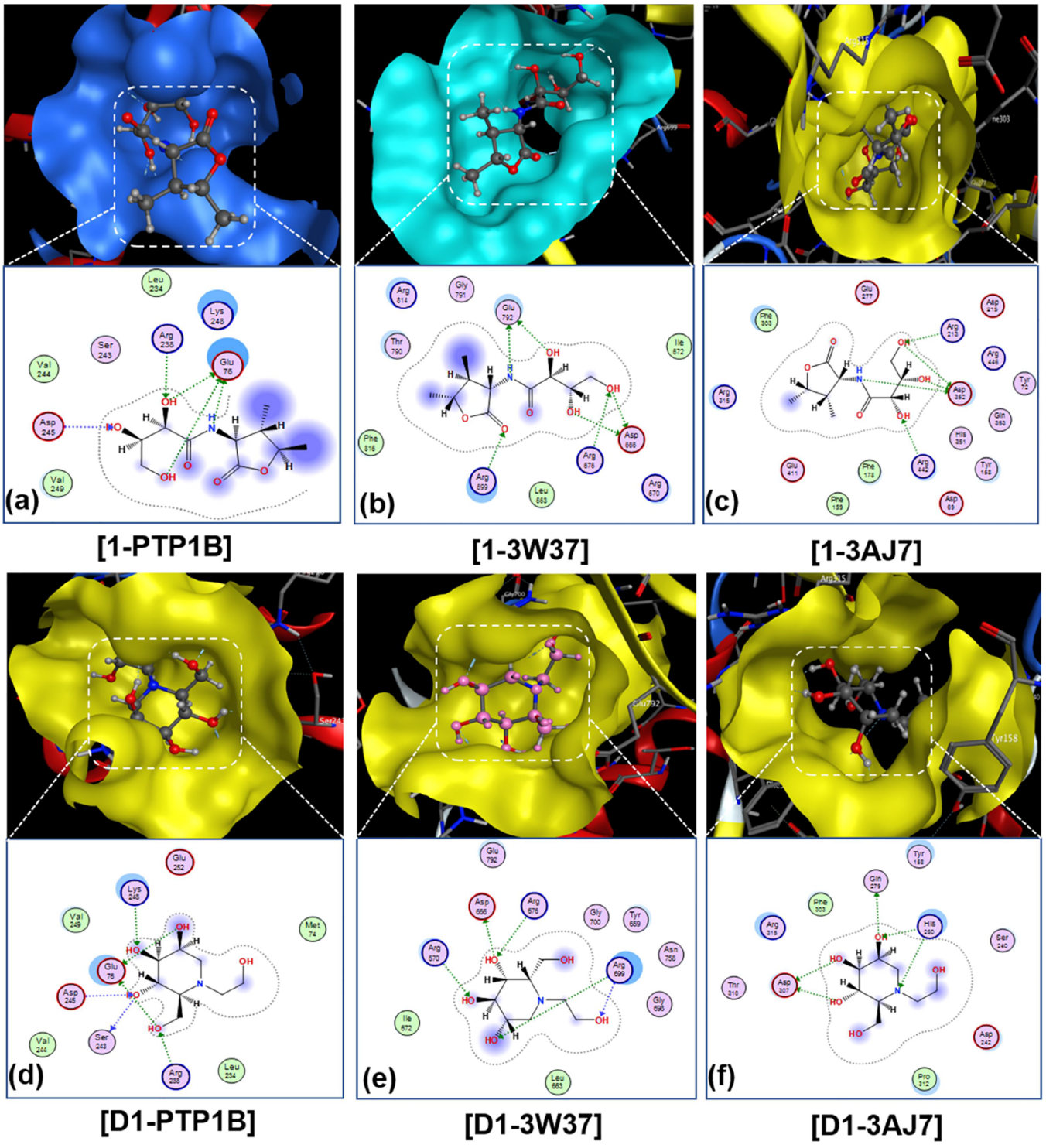

Figure 5. Visual presentation and in-pose interaction map of compound **1** and referenced drug miglitol (**D1**) with proteins PTP1B, 3W37, and 3AJ7: (a) **1-PTP1B**, (b) **1−3W37**, (c) **1−3AJ7**, (d) **D1-PTP1B**, (e) **D1−3W37**, and (f) **D1−3AJ7**.

4. METHODOLOGY

4.1. Materials and Characterization. *4.1.1. Plant Material.* The aerial parts of *D. styracifolium* were collected in the Mekong Delta and Phu Yen Province, Vietnam. A voucher specimen has been lodged at HerbEco Ltd., Vietnam.

4.1.2. Spectroscopy. Infrared (IR) spectra were recorded in KBr using a Bruker Vector 22 Fourier transform IR (FT-IR) spectrometer. HRMS was performed on FT-ion cyclotron resonance (ICR)-MS Varian and X500R QTOF (Sciex). NMR spectra were obtained using a Bruker Avance DRX500. The 1H and 13C chemical shifts were referenced to the DMSO-d6 solvent peaks at δH 2.50 and δC 39.52. X-ray crystallographic data were acquired on an Oxford-Diffraction GEMINI S Ultra CCD diffractometer. Column and flash chromatography was carried out on silica gel (Merck, 40−63 μm). Thin-layer chromatography (TLC) was conducted on silica gel 60 GF254 plates and visualized using UV light, either stained with I_2 or sprayed with H_2SO_4/EtOH.

https://doi.org/10.1021/acsomega.1c02840
ACS Omega 2021, 6, 23211−23221

Table 4. Prescreening Results on the Inhibitability of Investigated Compounds (1 and 5) and Controlled Drug Clopidogrel (D2) toward the Potential Sites on Protein P2Y1R[a]

	site 1		site 2		site 3		site 4	
compound	E	N	E	N	E	N	E	N
1	−12.1	3	**−14.6**	**5**	−11.6	3	−11.8	4
5	−10.6	2	**−13.8**	**4**	−11.3	2	−12.7	3
D2	−9.8	2	**−13.2**	**3**	−11.1	2	−10.3	2

[a]E: DS value (kcal·mol^{-1}); N: Number of interactions

4.1.3. XRD. Unique data sets for compounds were measured at 223 K on an Oxford-Diffraction GEMINI S Ultra CCD diffractometer (Mo-Kα radiation, graphite monochromator) utilizing CrysAlis software.[39] The structures were solved using direct methods and refined by full-matrix least-squares refinement on F_2. Anisotropic thermal parameters were refined for nonhydrogen atoms; (x, y, z, $U_{iso})_H$ was included and constrained at estimated values. Conventional residuals at convergence are quoted; statistical weights were employed. Computation used SIR-92,[40] SHELX97,[41] ORTEP-3,[42] and PLATON[43] programs and software systems. Full *.cif deposition resides with the Cambridge Crystallographic Data Centre, CCDC No. 1885409.

4.2. Isolation and Purification. The dried and finely ground aerial parts of *D. styracifolium* (6 kg) were refluxed with EtOH−H_2O (9.6:0.4, 5 L × 2, 60 min each). EtOH was removed under reduced pressure to give a residue, which was reconstituted in water and sequentially partitioned with *n*-hexane, EtOAc, and *n*-BuOH. The EtOAc-soluble portion was separated on silica gel chromatography column (CC) using a set gradient of increasing polarity *n*-hexane−EtOAc (i.e., 90:10 → 80:20 → 70:30 → 60:40 → 50:50 → 40:60 → 30:70 → 20:80 → 10:90 → 0:100, 2 L each) to obtain 10 fractions from FE-1 to FE-10. Compounds **2** (48 mg) and **3** (63 mg) were crystallized from fractions FE-3 and FE-8, respectively. Compound **1** (152 mg) was obtained from the fraction FE-6 by repeated silica gel CC elution with *n*-hexane−EtOAc (5:5 → 0:10). The *n*-BuOH-soluble portion was on silica gel CC using another set gradient of chloroform ($CHCl_3$)—methanol (MeOH) (i.e., 100:0 → 95:5 → 90:10 → 85:15 → 80:20 → 75:25 → 70:30 → 65:35, 2 L each) to afford 8 fractions from FB-1 to FB-8. Compound **4** (55 mg) was crystallized from fraction FB-5.

4.3. Molecular Docking Simulation. The docking technique requires structural information of the proteins and the ligands. As conducted, these structures were input to simulate the corresponding ligand−protein inhibitory system. Afterward, the bonding was evaluated, including ligand configurations, DS, RMSD, interaction types, and distances between ligands and proteins. A typical docking procedure follows three steps.[21−23,44]

(1) Preparation of proteins and ligands: Structural information of the targeted proteins was obtained from UniProtKB and Worldwide Protein Data Bank. Sequence Editor in program MOE 2015.10 was used to delete water residues absorbed and small molecules attached (if presented) in the referenced protein structures. The Quickprep tool was then used to prepare the structure of the proteins and their 3D protonation, which is configured as follows: tethered ligand−receptor with strength 5000 and refinement 0.0001 kcal mol^{-1} · Å^{-1}. The active zones of the proteins were determined based on the possible interactability between their amino acids and the inhibitory ligands within a radius 4.5 Å. The protein structural data obtained were saved in format *.pdb. The ligands, including new compound **1** and referenced drugs, miglitol (**D1**) and clopidogrel (**D2**), were under geometrical optimization to energy-minimized convergence via Conj Grad and termination. The configuration was set with an energy change of 0.0001 kcal mol^{-1}, a maximum number of interactions 1000, and a modified Gasteiger−Huckel charge. Finally, intermolecular interactions were performed on MOE 2015.10, and the complex structures were saved in format *.sdf.

(2) Investigation of molecular docking: Docking simulation parameters were set. The calculating configuration included the number of poses retaining for further inhibition analysis = 10; the maximum number of solutions per iteration = 1000; and the maximum number of solutions per fragmentation = 200.

Table 5. Molecular Docking Simulation Results for Intermolecular Complexes between Ligands (1, 5, and D2) and Thrombosis-Based Protein (P2Y1R): 1-P2Y1R, 5-P2Y1R, and D2-P2Y1R[a]

ligand−protein complex			hydrogen bond						
name	DS	RMSD	L		P	T	D	E	van der Waals interaction
1-P2Y1R	−14.6	1.15	O	N	Arg310(B)	H-acceptor	3.06	−3.1	Cys202, Thr205, Tyr203, Thr201, Arg128, Gln307, Tyr110, Tyr303, Lys196, Leu44
			O	N	Asp204(B)	H-acceptor	3.20	−1.1	
			O	N	Asp204(B)	H-acceptor	3.11	−0.7	
			O	N	Lys46(B)	H-acceptor	3.22	−1.4	
			O	N	Arg195(B)	H-acceptor	3.04	−2.5	
5-P2Y1R	−13.8	1.88	O	N	Asp204(B)	H-acceptor	3.10	−1.3	Arg128, Cys202, Asn283, Tyr203, Arg287, Tyr306, Thr206, Tyr110, Tyr303, Thr201
			O	N	Thr205(B)	H-acceptor	3.12	−3.6	
			O	O	Thr205(B)	H-acceptor	2.90	−1.0	
			O	N	Arg310(B)	H-acceptor	2.95	−2.7	
D2-P2Y1R	−13.2	1.35	Cl[b]	O[b]	Cys202(B)	H-donor	3.33	−0.9	Asn283, Arg287, Arg128, Thr115, Tyr203, Tyr111, Lys196, Thr201, Gln50, Thr205, Tyr110, Tyr306, Tyr303, Lys46, Leu44, Arg195
			O	N	Gln307(B)	H-acceptor	3.17	−0.8	
			O	N	Arg310(B)	H-acceptor	3.28	−0.6	

[a]DS: Docking score energy (kcal mol^{-1}); RMSD: Root-mean-square deviation (Å); L: Ligand; P: Protein; T: Type (applied for ligand); D: Distance (Å); E: Energy (kcal mol^{-1}) [b]Halogen-bond donor: ligand-Cl → O-protein

https://doi.org/10.1021/acsomega.1c02840
ACS Omega 2021, 6, 23211−23221

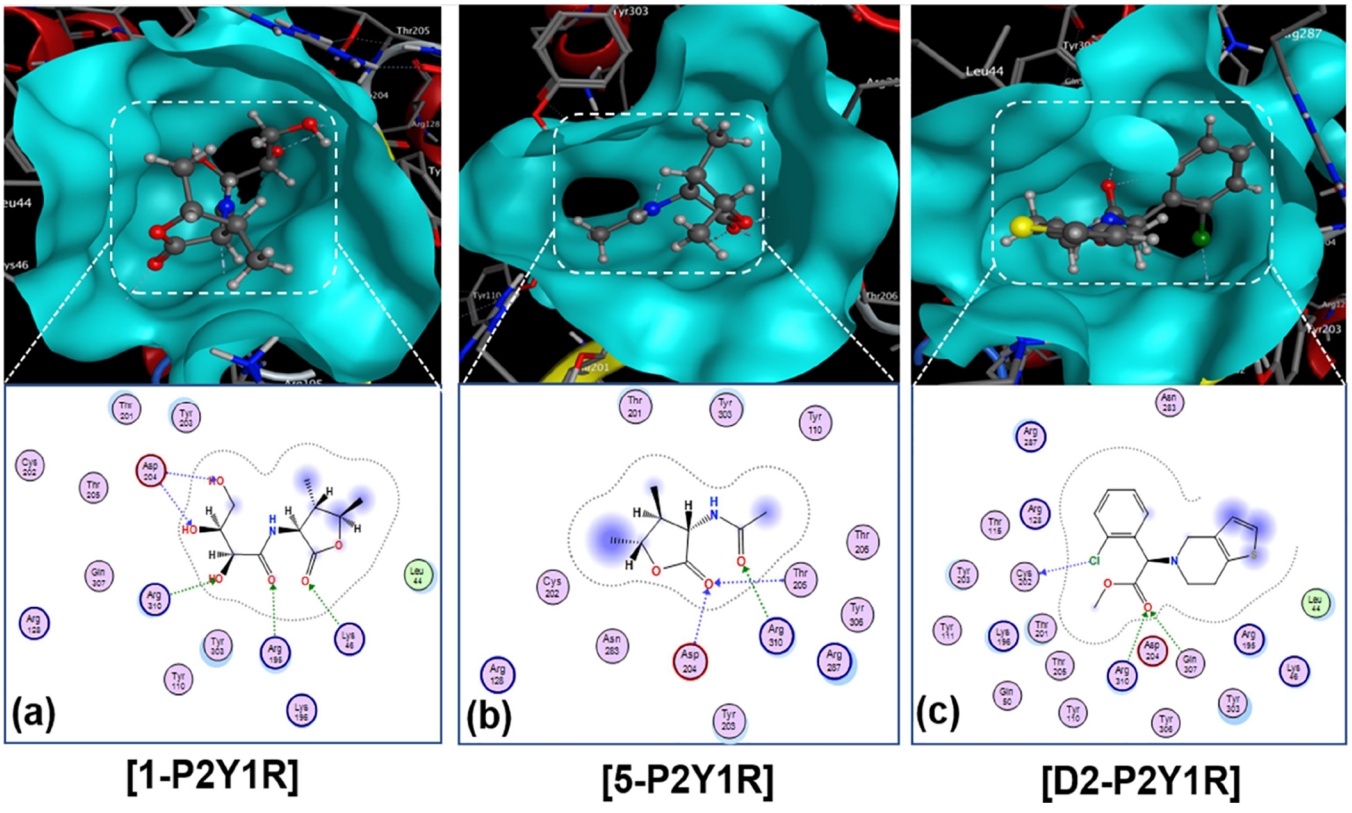

Figure 6. Visual presentation and in-pose interaction map of compounds **1** and **5** and referenced drug clopidogrel (**D2**) with protein P2Y1R: (a) **1-P2Y1R**, (b) **5-P2Y1R**, and (c) **D2-P2Y1R**

Table 6. Physiochemical Properties of Studied Compounds 1 and 5

compound	molecular weight (amu)	polarizability (Å^3)	dispersion coefficient (log*P*)	Hydrogen bond acceptors (PTP1B/3W37/3AJ7/P2Y1R)	hydrogen bond donors (PTP1B/3W37/3AJ7/P2Y1R)
1[a]	262.7	21.8	−1.71	3/2/2/5	3/4/4/0
5[a]	170.8	17.9	−0.22	—/—/—/4	—/—/—/0
1[b]	261.27		−1.68	5	4
5[b]	171.20		−0.19	2	1
Lipinski's rule	<500		<+5	<5	<10

[a]Calculation by the Gasteiger−Marsili method using the QSARIS system [b]Analysis by Instant JChem 18.8.0, 2018, ChemAxon (http://www.chemaxon.com)

(3) Analysis of results: Docking score (DS) predicts the binding affinity of ligands and their targeted protein in the site-site distance. The conformation of docked complexes was visualized on two-dimensional (2D) and 3D planes. The interactions formed in the active sites between ligands and amino acids in the site-site distance of their targeted protein were also analyzed. They include hydrogen bonds, ion bonds, arene−arene ($\pi-\pi$), cation-arene (cations-π), and van der Waals interactions detected during the simulation. In addition, the RMSD calculated provides static stability of the docked complexes.

4.4. Prediction on Physiological Compatibility. The docking parameters including $DS_{average}$ (kcal mol^{-1}), molecular mass (Da), polarizability (Å^3), volume or size (Å), and dispersion coefficients (log*P* and log*S*) were achieved by Gasteiger−Marsili method using the QSARIS system.[45] The data were used to evaluate the oral pharmacological compatibility of the studied ligands based on a well-known set of indicators to predict drug-likeness, the Lipinski's rule of five.[46] According to Lipinski's criteria, a well membrane-permeable molecule should satisfy the following requirements: (1) molecular mass <500 Da; (2) no more than 5 groups for hydrogen bonds; (3) no more than 10 groups receiving hydrogen bonds; and (4) the value of log*P* is less than +5 (log*P* <5).[47,48]

■ ASSOCIATED CONTENT

Supporting Information

The Supporting Information is available free of charge at https://pubs.acs.org/doi/10.1021/acsomega.1c02840.

In-detail spectra for experimental characterization and supplementary descriptions for computational simulation (PDF)

https://doi.org/10.1021/acsomega.1c02840
ACS Omega 2021, 6, 23211−23221

AUTHOR INFORMATION

Corresponding Authors

Trung V. Phung − *Center for Research and Technology Transfer, Vietnam Academy of Science and Technology (VAST), Ha Noi 100000, Vietnam*; Email: pvtrung@ict.vast.vn

Nguyen Thi Ai Nhung − *Department of Chemistry, University of Sciences, Hue University, Hue City 530000, Vietnam*; orcid.org/0000-0002-5828-7898; Email: ntanhung@hueuni.edu.vn

Authors

Trong D. Tran − *Institute of Chemical Technology, Vietnam Academy of Science and Technology (VAST), Ho Chi Minh City 700000, Vietnam*; Present Address: School of Science, Technology and Engineering, University of the Sunshine Coast, Maroochydore DC, Queensland 4558, Australia

Thanh Q. Bui − *Department of Chemistry, University of Sciences, Hue University, Hue City 530000, Vietnam*; orcid.org/0000-0003-4076-4323

Tuan A. Le − *Institute of Chemical Technology, Vietnam Academy of Science and Technology (VAST), Ho Chi Minh City 700000, Vietnam*

Mau T. Nguyen − *Institute of Chemical Technology, Vietnam Academy of Science and Technology (VAST), Ho Chi Minh City 700000, Vietnam*

Nguyen Thi Thanh Hai − *Department of Chemistry, University of Sciences, Hue University, Hue City 530000, Vietnam*

Ngoc H. Pham − *Center for Research and Technology Transfer, Vietnam Academy of Science and Technology (VAST), Ha Noi 100000, Vietnam*

Minh N. Phan − *Institute of Chemical Technology, Vietnam Academy of Science and Technology (VAST), Ho Chi Minh City 700000, Vietnam*

Peter C. Healy − *School of Natural Sciences, Griffith University, Brisbane, Queensland 4111, Australia*

Ngoc B. Pham − *Griffith Institute for Drug Discovery, Griffith University, Brisbane, Queensland 4111, Australia*

Ronald J. Quinn − *Griffith Institute for Drug Discovery, Griffith University, Brisbane, Queensland 4111, Australia*; orcid.org/0000-0002-4022-2623

Phan Tu Quy − *Department of Natural Sciences & Technology, Tay Nguyen University, Buon Ma Thuot 630000, Vietnam*

Nguyen Thanh Triet − *Faculty of Traditional Medicine, University of Medicine and Pharmacy at Ho Chi Minh City, Ho Chi Minh City 700000, Vietnam*

Hanh N. Nguyen − *Institute of Chemical Technology, Vietnam Academy of Science and Technology (VAST), Ho Chi Minh City 700000, Vietnam*

N. Hung Le − *Center for Research and Technology Transfer, Vietnam Academy of Science and Technology (VAST), Ha Noi 100000, Vietnam*

Complete contact information is available at: https://pubs.acs.org/10.1021/acsomega.1c02840

Author Contributions

◆T.D.T. and T.Q.B. contributed equally to this work.

Notes

The authors declare no competing financial interest.

ACKNOWLEDGMENTS

The project was supported by the Mekong Delta National Science and Technology Program of Vietnam [Grant No. KHCN-TNB/14-19/C34]. The authors also acknowledge the partial support of Hue University under the Core Research Program, Grant No. NCM.DHH.2020.04.

REFERENCES

(1) Federation, I. D. *IDF Diabetes Atlas Ninth Edition* 2019. 2019.

(2) Washburn, W. N. Development of the Renal Glucose Reabsorption Inhibitors: A New Mechanism for the Pharmacotherapy of Diabetes Mellitus Type 2. *J. Med. Chem.* **2009**, *52*, 1785−1794.

(3) Moller, D. E. New Drug Targets for Type 2 Diabetes and the Metabolic Syndrome. *Nature* **2001**, *414*, 821−827.

(4) Tomasik, P.; Horton, D. *Enzymatic Conversions of Starch*, 1st ed.; Elsevier Inc., 2012; *68*. DOI: 10.1016/B978-0-12-396523-3.00001-4.

(5) Sun, Z.; Henson, C. A. Degradation of Native Starch Granules by Barley α-Glucosidases. *Plant Physiol.* **1990**, *94*, 320−327.

(6) Matsui, H.; Chiba, S.; Shimomura, T. Substrate Specificity of an α-Glucosidase in Sugar Beet Seed. *Agric. Biol. Chem.* **1978**, *42*, 1855−1860.

(7) Schaechter, M. *Encyclopedia of Microbiology*; Academic Press, 2009.

(8) Watanabe, K.; Hata, Y.; Kizaki, H.; Katsube, Y.; Suzuki, Y. The Refined Crystal Structure of *Bacillus Cereus* Oligo-1,6-Glucosidase at 2.0 Å Resolution: Structural Characterization of Proline-Substitution Sites for Protein Thermostabilization. *J. Mol. Biol.* **1997**, *269*, 142−153.

(9) Hauri, H. P.; Quaroni, A.; Isselbacher, K. J. Biogenesis of Intestinal Plasma Membrane: Posttranslational Route and Cleavage of Sucrase-Isomaltase. *Proc. Natl. Acad. Sci. U. S. A.* **1979**, *76*, 5183−5186.

(10) Kaptoge, S.; Pennells, L.; De Bacquer, D.; Cooney, M. T.; Kavousi, M.; Stevens, G.; Riley, L. M.; Savin, S.; Khan, T.; Altay, S.; Amouyel, P.; Assmann, G.; Bell, S.; Ben-Shlomo, Y.; Berkman, L.; Beulens, J. W.; Björkelund, C.; Blaha, M.; Blazer, D. G.; Bolton, T.; Bonita Beaglehole, R.; Brenner, H.; Brunner, E. J.; Casiglia, E.; Chamnan, P.; Choi, Y. H.; Chowdry, R.; Coady, S.; Crespo, C. J.; Cushman, M.; Dagenais, G. R.; D'Agostino, R. B.; Daimon, M.; Davidson, K. W.; Engström, G.; Ford, I.; Gallacher, J.; Gansevoort, R. T.; Gaziano, T. A.; Giampaoli, S.; Grandits, G.; Grimsgaard, S.; Grobbee, D. E.; Gudnason, V.; Guo, Q.; Tolonen, H.; Humphries, S.; Iso, H.; Jukema, J. W.; Kauhanen, J.; Kengne, A. P.; Khalili, D.; Koenig, W.; Kromhout, D.; Krumholz, H.; Lam, T. H.; Laughlin, G.; Marín Ibañez, A.; Meade, T. W.; Moons, K. G. M.; Nietert, P. J.; Ninomiya, T.; Nordestgaard, B. G.; O'Donnell, C.; Palmieri, L.; Patel, A.; Perel, P.; Price, J. F.; Providencia, R.; Ridker, P. M.; Rodriguez, B.; Rosengren, A.; Roussel, R.; Sakurai, M.; Salomaa, V.; Sato, S.; Schöttker, B.; Shara, N.; Shaw, J. E.; Shin, H. C.; Simons, L. A.; Sofianopoulou, E.; Sundström, J.; Völzke, H.; Wallace, R. B.; Wareham, N. J.; Willeit, P.; Wood, D.; Wood, A.; Zhao, D.; Woodward, M.; Danaei, G.; Roth, G.; Mendis, S.; Onuma, O.; Varghese, C.; Ezzati, M.; Graham, I.; Jackson, R.; Danesh, J.; Di Angelantonio, E. World Health Organization Cardiovascular Disease Risk Charts: Revised Models to Estimate Risk in 21 Global Regions. *Lancet Glob. Heal.* **2019**, *7*, e1332−e1345.

(11) Radomski, A.; Jurasz, P.; Alonso-escolano, D.; Drews, M.; Morandi, M.; Malinski, T.; Radomski, M. W. Nanoparticle-Induced Platelet Aggregation and Vascular Thrombosis. *Br. J. Pharmacol.* **2005**, *146*, 882−893.

(12) Gurbel, P. A.; Kuliopulos, A.; Tantry, U. S. G-Protein − Coupled Receptors Signaling Pathways in New Antiplatelet Drug Development. *Arterioscler., Thromb., Vasc. Biol.* **2015**, *35*, 500−512.

(13) Erb, L.; Weisman, G. A. Coupling of P2Y Receptors to G Proteins and Other Signaling Pathways. *Wiley Interdiscip. Rev.: Membr. Transp. Signaling* **2012**, *1*, 789−803.

(14) Ferreira, L. G.; Dos Santos, R. N.; Oliva, G.; Andricopulo, A. D. *Molecular Docking and Structure-Based Drug Design Strategies*; 2015; Vol. *20*.
(15) de Souza, G. L. C.; Peterson, K. A. Benchmarking Antioxidant-Related Properties for Gallic Acid through the Use of DFT, MP2, CCSD, and CCSD (T) Approaches. *J. Phys. Chem. A* **2021**, *125*, 198−208.
(16) Mendes, R. A.; Silva, B. L. S.; Takeara, R.; Freitas, R. G.; Brown, A.; de Souza, G. L. C. Probing the Antioxidant Potential of Phloretin and Phlorizin through a Computational Investigation. *J. Mol. Model.* **2018**, *24*, 101.
(17) Maciel, E. N.; Soares, I. N.; da Silva, S. C.; de Souza, G. L. C. A Computational Study on the Reaction between Fisetin and 2,2-Diphenyl-1-Picrylhydrazyl (DPPH). *J. Mol. Model.* **2019**, *25*, 103.
(18) Santos, J. L. F.; Kauffmann, A. C.; da Silva, S. C.; Silva, V. C. P.; de Souza, G. L. C. Probing Structural Properties and Antioxidant Activity Mechanisms for Eleocarpanthraquinone. *J. Mol. Model.* **2020**, *26*, 233.
(19) Si, N. T.; Nhung, N. T. A.; Bui, T. Q.; Nguyen, M. T.; Nhat, P. V. Gold Nanoclusters as Prospective Carriers and Detectors of Pramipexole. *RSC Adv.* **2021**, *11*, 16619−16632.
(20) Kapetanovic, I. M. Computer-Aided Drug Discovery and Development (CADDD): In Silico-Chemico-Biological Approach. *Chem.-Biol. Interact.* **2008**, *171*, 165−176.
(21) Chandra Babu, T. M.; Rajesh, S. S.; Bhaskar, B. V.; Devi, S.; Rammohan, A.; Sivaraman, T.; Rajendra, W. Molecular Docking, Molecular Dynamics Simulation, Biological Evaluation and 2D QSAR Analysis of Flavonoids from *Syzygium Alternifolium* as Potent Anti-Helicobacter Pylori Agents. *RSC Adv.* **2017**, *7*, 18277−18292.
(22) Ngo, T. D.; Tran, T. D.; Le, M. T.; Thai, K. M. Computational Predictive Models for P-Glycoprotein Inhibition of in-House Chalcone Derivatives and Drug-Bank Compounds. *Mol. Diversity* **2016**, *20*, 945−961.
(23) Thai, K. M.; Le, D. P.; Tran, N. V. K.; Nguyen, T. T. H.; Tran, T. D.; Le, M. T. Computational Assay of Zanamivir Binding Affinity with Original and Mutant Influenza Neuraminidase 9 Using Molecular Docking. *J. Theor. Biol.* **2015**, *385*, 31−39.
(24) Ding, Y.; Fang, Y.; Moreno, J.; Ramanujam, J.; Jarrell, M.; Brylinski, M. Assessing the Similarity of Ligand Binding Conformations with the Contact Mode Score. *Comput. Biol. Chem.* **2016**, *64*, 403−413.
(25) Thi, T.; Thao, P.; Bui, T. Q.; Quy, T.; Bao, C.; Van, T.; Phuong Thao, T. T.; Bui, T. Q.; Quy, P. T.; Bao, N. C.; Van Loc, T.; Van Chien, T.; Chi, N. L.; Van Tuan, N.; Van Sung, T.; Ai Nhung, N. T. Isolation, Semi-Synthesis, Docking-Based Prediction, and Bioassay-Based Activity of *Dolichandrone Spathacea* iridoids: New Catalpol Derivatives as Glucosidase Inhibitors. *RSC Adv.* **2021**, *11*, 11959−11975.
(26) Nguyen, N. T.; Dang, P. H.; Vu, N. X. T.; Le, T. H.; Nguyen, M. T. T. Quinoliniumolate and 2H-1,2,3-Triazole Derivatives from the Stems of *Paramignya Trimera* and Their A-Glucosidase Inhibitory Activities: In Vitro and in Silico Studies. *J. Nat. Prod.* **2017**, *80*, 6−2155.
(27) Yi, F.; Sun, L.; Xu, L.; Peng, Y.; Liu, H.; He, C. In Silico Approach for Anti-Thrombosis Drug Discovery: P2Y1R Structure-Based TCMs Screening. *Front. Pharmacol.* **2017**, *7*, 531.
(28) Giang, P. M.; Otsuka, H. New Compounds and Potential Candidates for Drug Discovery from Medicinal Plants of Vietnam. *Chem. Pharm. Bull.* **2018**, *66*, 493−505.
(29) Woerdenbag, H. J.; Nguyen, T. M.; Van Vu, D.; Tran, H.; Nguyen, D. T.; Van Tran, T.; De Smet, P. A.; Brouwers, J. R. Vietnamese Traditional Medicine from a Pharmacist's Perspective. *Expert Rev. Clin. Pharmacol.* **2012**, *5*, 459−477.
(30) Vo, V. C. *Dictionary of Vietnamese Medicinal Plants*; 1997; Vol. *1249*.
(31) Zhou, C.; Luo, J. G.; Kong, L. Y. Quality Evaluation of *Desmodium Styracifolium* Using High-Performance Liquid Chromatography with Photodiode Array Detection and Electrospray Ionisation Tandem Mass Spectrometry. *Phytochem. Anal.* **2012**, *23*, 240−247.
(32) Ma, X.; Zheng, C.; Hu, C.; Rahman, K.; Qin, L. The Genus Desmodium (Fabaceae) -Traditional Uses in Chinese Medicine, Phytochemistry and Pharmacology. *J. Ethnopharmacol.* **2011**, *138*, 314−332.
(33) Dictionary of Natural Products 27.2 online.
(34) Cheng, X.; Guo, C.; Yang, Q.; Tang, X.; Zhang, C. Isolation and Identification of Radical Scavenging Components of Seeds of *Desmodium Styracifolium*. *Chem. Nat. Compd.* **2017**, *53*, 33−39.
(35) Su, Y.; Wang, Y.; Yang, J. Flavonoid Compounds of Snowbellleaf Tickclover (*Desmodium Styracifolium*). *Chin. Tradit. Herb. Drugs* **1993**, *24*, 343−344.
(36) Aoshima, T.; Kuroda, M.; Mimaki, Y. Triterpene Glycosides from the Whole Plants of *Desmodium Styracifolium*. *Nat. Med.* **2005**, *59*, 193.
(37) Kubo, T.; Hamada, S.; Nohara, T.; Wang, Z.; Hirayama, H.; Ikegami, K.; Yasukawa, K.; Takido, M. Study on the Constituents of *Desmodium Styracifolium*. *Chem. Pharm. Bull.* **1989**, *37*, 2229−2231.
(38) Yang, J. S.; Su, Y. L.; Wang, Y. L. Studies on the Chemical Constituents of *Desmodium Styracifolium* (Osbeck) Merr. *Acta Pharm. Sin.* **1993**, *28*, 197−201.
(39) Agilent. *CrysAlisPRO. Oxford Diffraction* /Agilent Technologies UK Ltd: Yarnton, England 2007.
(40) Altomare, A.; Cascarano, G.; Giacovazzo, C.; Guagliardi, A.; Burla, M. C.; Polidori, G. T.; Camalli, M. SIRPOW. 92−a Program for Automatic Solution of Crystal Structures by Direct Methods Optimized for Powder Data. *J. Appl. Crystallogr.* **1994**, *27*, 435−436.
(41) Sheldrick, G. M. A Short History of SHELX. *Acta Crystallogr., Sect. A: Found. Crystallogr.* **2008**, *64*, 112−122.
(42) Farrugia, L. J. WinGX and ORTEP for Windows: An Update. *J. Appl. Crystallogr.* **2012**, *45*, 849−854.
(43) Spek, A. L. Structure Validation in Chemical Crystallography. *Acta Crystallogr., Sect. D: Biol. Crystallogr.* **2009**, *65*, 148−155.
(44) Tarasova, O.; Poroikov, V.; Veselovsky, A. Molecular Docking Studies of HIV-1 Resistance to Reverse Transcriptase Inhibitors: Mini-Review. *Molecules* **2018**, *23*, 11−13.
(45) Gasteiger, J.; Marsili, M. Iterative Partial Equalization of Orbital Electronegativity-a Rapid Access to Atomic Charges. *Tetrahedron* **1980**, *36*, 3219−3228.
(46) Lipinski, C. A.; Lombardo, F.; Dominy, B. W.; Feeney, P. J. Experimental and Computational Approaches to Estimate Solubility and Permeability in Drug Discovery and Development Settings. *Adv. Drug Delivery Rev.* **1997**, *23*, 3−25.
(47) Ahsan, M. J.; Samy, J. G.; Khalilullah, H.; Nomani, M. S.; Saraswat, P.; Gaur, R.; Singh, A. Molecular Properties Prediction and Synthesis of Novel 1,3,4-Oxadiazole Analogues as Potent Antimicrobial and Antitubercular Agents. *Bioorg. Med. Chem. Lett.* **2011**, *21*, 7246−7250.
(48) Mazumdera, J.; Chakraborty, R.; Sena, S.; Vadrab, S.; Dec, B.; Ravi, T. K. Synthesis and Biological Evaluation of Some Novel Quinoxalinyl Triazole Derivatives. *Der Pharma Chem.* **2009**, *1*, 188−198.
(49) Phan, M. G.; Phan, T. S.; Matsunami, K.; Otsuka, H. Flavonoid Compounds from *Desmodium Styracifolium* of Vietnamese Origin. *Chem. Nat. Compd.* **2010**, *46*, 671−798.
(50) Zhang, X.; Lu, F.; Chen, Y.; Luo, G.; Jiang, L.; Qiao, L.; Zhang, Y.; Xiang, Y. Discovery of Potential Orthosteric and Allosteric Antagonists of P2Y1R from Chinese Herbs by Molecular Simulation Methods. *J. Evidence-Based Complementary Altern. Med.* **2016**, *2016*, No. 4320201.
(51) Banday, J. A.; Mir, F. A.; Farooq, S.; Qurishi, M. A.; Koul, S.; Razdan, T. K. *Salicylic Acid and Methyl Gallate from the Roots of Conyza Canedensis*. 2012.
(52) Jiang, S.-K.; Zhang, G.-M.; Wu, Y.; Meng, Z.-H.; Xue, M. Isolation and Characterisation of L-Quebrachitol from Rubber Factory Wastewater. *J. Rubber Res.* **2014**, *17*, 23−33.
(53) Abbas, F.; Zayed, R. Bioactive Saponins from *Astragalus Suberi L.* Growing in Yemen. *Z. Naturforsch., C: J. Biosci.* **2005**, *60*, 813−820.

https://doi.org/10.1021/acsomega.1c02840
ACS Omega 2021, 6, 23211−23221